Ferroelectrics, 376:122–128, 2008

ISSN: 0015-0193 print / 1563-5112 online
DOI: 10.1080/00150190802440948

Taylor & Francis
Taylor & Francis Group

Ferroelectric Domain Structures in $BiFeO_3$-$BaTiO_3$

S. KITAGAWA,[1] T. OZAKI,[2] Y. HORIBE,[3] K. YOSHII,[4] AND S. MORI[2,*]

[1]Department of Physics, Osaka Prefecture University, Sakai, Osaka 599-8531 Japan
[2]Department of Materials Science, Osaka Prefecture University, Sakai, Osaka 599-8531, Japan
[3]Department of Physics and Astronomy, Rutgers University, Piscataway, NJ 08854, U.S.A.
[4]Japan Atomic Energy Agency, Hyogo 679-5148, Japan

Microstructures associated with the ferroelectric (FE) properties in (1-x)$BiFeO_3$-x$BaTiO_3$ were investigated mainly by a transmission electron microscopy. It was found that large FE domains in $BiFeO_3$ changed into complicated FE microdomains with the 20–30 nm width in the $x = 0.25$ compound. The directions of the spontaneous polarization in each FE microdomains were determined by obtaining dark-field images. Changes of the FE microdomains for $x = 0.28$ composition as a function of the temperature were also investigated.

Keywords Multiferroic materials; ferroelectric domain; electron diffraction

PACS numbers: 77.80.-e; 61.05.J- ; 68.37.Lp; 75.60.Ch

1. Introduction

Magnetic ferroelectrics (the so-called multiferroic materials) have attracted renewed interest recently because of their potential in novel magneto-electric and magneto-optical devices [1–3]. In magnetic ferroelectrics, both magnetic and ferroelectric (FE) orderings are involved with local spins and an off-center structural distortion, respectively. These two seemingly unrelated phenomena can coexist in magnetic ferroelectrics [4–6]. In addition, the mutual control of magnetization and electric polarization can be accomplished in hexagonal manganites such as $TbMnO_3$ and $HoMnO_3$ [7–9]. A recent work by Zhao et al. succeeded in observing the electrical control of the antiferromagnetic domain structure in multiferroic $BiFeO_3$ thin films by using the piezo force microscopy, combined with the X-ray photoemission electron microscopy [10].

$BiFeO_3$ is one of the typical multiferroic materials, in which ferroelectricity and antiferromagnetism coexist at room temperature [11–13]. Some previous works have reported that $BiFeO_3$ exhibits a structural phase transition from the rhombohedral structure (space group $R3c$) to the cubic one around $T_C \sim 1110$ K, which accompanies the polar displacement of

Received March 1, 2008; in final form July 2, 2008.
*Corresponding author. E-mail: mori@mtr.osakafu-u.ac.jp

the Bi, Fe and O ions along the [111] direction and the cooperative rotation of the FeO_6 octahedra around the [111] axis. The cubic-to-rhombohedral transition accompanies the appearance of the spontaneous polarization (P_s) along the [111] direction. Note that the high-temperature paraelectric structure with the cubic symmetry has not been determined correctly. Subsequently an antiferromagnetic transition occurs at T_N ~650 K. From these results, $BiFeO_3$ exhibits the coexisting state of the FE and antiferromagnetic orders at room temperature. It has been reported recently that the magnitude of P_s is enhanced dramatically in $BiFeO_3$ thin films with the tetragonal structure (space group: *P4mm*) [3]. This experimental result suggested that the decrease of the rhombohedral distortion along the [111] direction has close relation to the enhancement of the ferroelectricity [3]. Theoretical consideration by using accurate density functional calculations suggests that large P_s comes from the hybridization interaction between Bi-O and Fe-O bonds [14]. The ferroelectricity in $BiFeO_3$ originates from the distortion of the Bi-O coordination environment as a result of the stereochemical activity of the lone pair on Bi.

On the other hand, it has been reported that (1-x)$BiFeO_3$-x$BaTiO_3$ has a structural phase transition from the rhombohedral structure to the cubic one around the $BaTiO_3$ concentration (x) of x = 0.33. In addition, anomalies in dielectric and magnetic susceptibilities were found around x = 0.33. This suggested that there is some close relationship between structural change and dielectric/magnetic properties in (1-x)$BiFeO_3$-x$BaTiO_3$ [15]. Thus, we have carefully investigated both microstructures and structural changes associated with the anomalies of dielectric/magnetic properties in (1-x)$BiFeO_3$-x$BaTiO_3$by a transmission electron microscope (TEM) experiments. Changes of the microstructures associated with the FE properties will be reported. In addition, the directions of P_s in each FE domains by taking dark-field images were determined on the basis of the experimental data.

2. Experimental

Polycrystalline samples of (1-x)$BiFeO_3$-x$BaTiO_3$ with x = 0.0, 0.20, 0.25, 0.28 and 0.35 were prepared by the conventional solid-state reaction method. The crystal structures of the obtained samples were checked by the x-ray diffraction method. In order to evaluate the magnetic and FE properties, we have measured both magnetic and FE hysteresis curves at room temperature. The crystallographic features of the obtained samples were examined by taking electron diffraction patterns and bright- and dark-field images. Observation was carried out between room temperature and 700 K, using a JEM-2010 TEM equipped with a heating holder. Specimens for the TEM observation were prepared by an Ar-ion thinning technique.

3. Experimental Results and Discussion

$BiFeO_3$ has a rhombohedrally distorted perovskite-type structure at room temperature as shown schematically in Fig. 1. Note that the space group is identified as *R3c*. The cooperative rotation of FeO_6 octahedra along the [111] direction, in addition to the polar displacements of Bi, Fe and O ions along the [111] direction, gives rise to the rhombohedral distortion in $BiFeO_3$. We have carefully investigated changes of the crystal structure by the increase of the $BaTiO_3$concentration in (1-x)$BiFeO_3$-x$BaTiO_3$ by obtaining various electron diffraction patterns at room temperature. Figure 2 shows the electron diffraction patterns in (1-x)$BiFeO_3$-x$BaTiO_3$with (a) x = 0.0, (b) 0.25, (c) 0.28 and (d) x = 0.35, respectively. Note that the electron beam incidence is almost parallel to the [1–10] direction. As indicated by

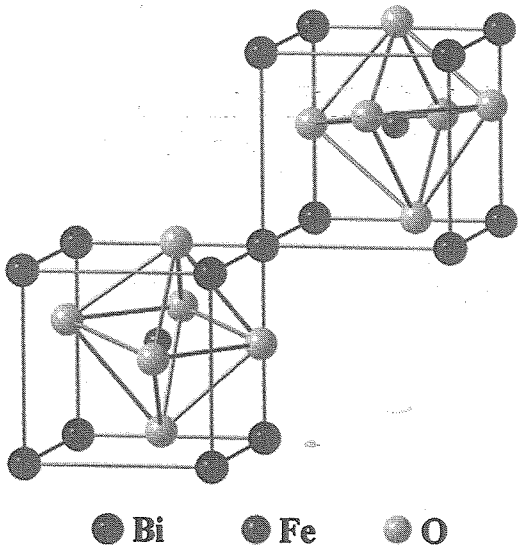

Figure 1. Crystal structure in the ferroelectric phase of $BiFeO_3$ at room temperature.

arrows in Figs. 2(a), 2(b) and 2(c), superlattice reflections at 1/2 1/2 1/2-type positions can be clearly seen in addition to the fundamental reflections due to the cubic perovskite-type structure. As understood by the comparison of the intensities of the superlattice reflections at 1/2 1/2 1/2 in Figs. 2(a), 2(b) and 2(c), these intensities for the composition x = 0.0 are

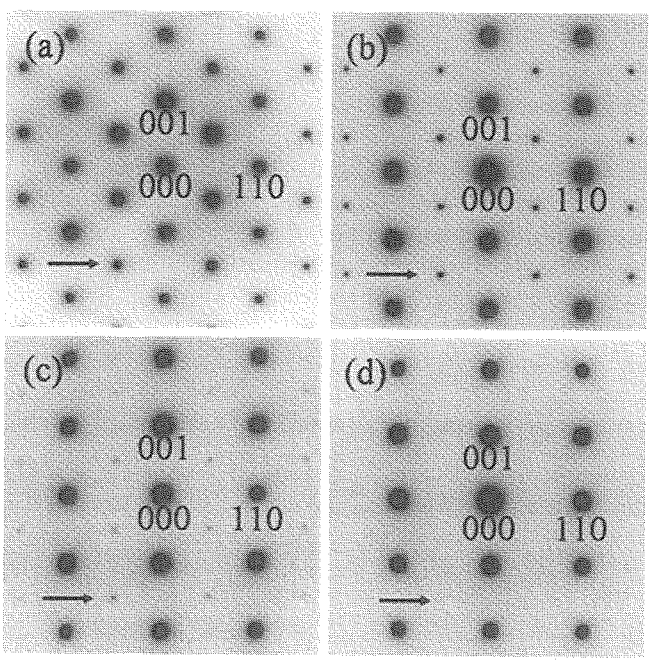

Figure 2. Electron diffraction patterns at room temperature with the [1-10] incidence in (a) x = 0.0, (b) 0.25, (c) 0.28 and (d) 0.35, respectively.

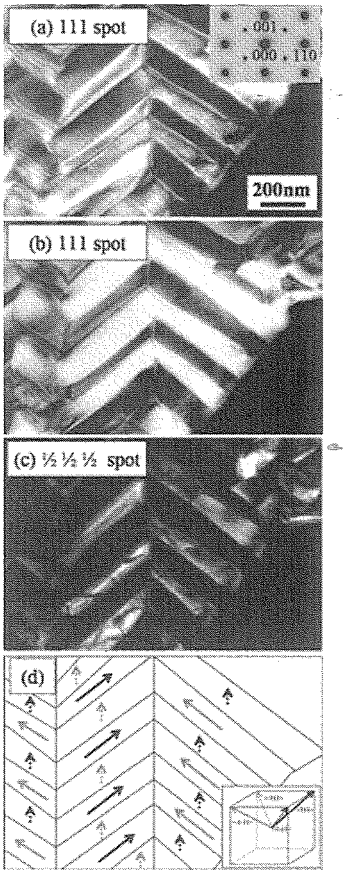

Figure 3. Ferroelectric domain structure in the x = 0.20 compound. (a) $g = [111]$, (b) tilted and (c) $g = [1/2\ 1/2\ 1/2]$. (d) Schematic description of the FE domain configuration determined in this work.

much stronger than those for the compositions x = 0.25 and x = 0.28. It should be noted that the rhombohedral distortion in these compounds is characterized as the presence of the superlattice reflection spots at 1/2 1/2 1/2-type positions. These reflections imply that the rhombohedral distortion in the x = 0.25 and 0.28 compounds is much smaller than that in the x = 0.0 compound. It is suggested that the magnitudes of the displacements of Bi, Fe and O ions along [111] direction decrease by substituting $BaTiO_3$ for $BiFeO_3$.

Changes of the microstructures related to the FE properties were investigated by obtaining the real-space images in (1-x)$BiFeO_3$-x$BaTiO_3$. As reported in the previous work [10], $BiFeO_3$ has large FE domains at room temperature. Note that domain structures due to the rhombohedrally distorted structure in $BiFeO_3$ correspond to the FE domain structures. Figure 3(a) displays the dark-field images obtained by using the 111 fundamental reflection spot at room temperature in the x = 0.20 composition. Note that the 111 fundamental reflection spot corresponds to $g = [111]$, where g denotes the reciprocal lattice vector. As can be understood in Fig. 3(a), the size of the FE domains reduce to the size of the $\sim 100 \mu$m. In order to determine the direction of P_s in each FE domains, we obtained dark-field images at room temperature by using various different g vectors. For instance, Figs. 3(b) and 3(c) exhibit the microstructures that were obtained by using $g = [111]$ and $g = [1/2\ 1/2\ 1/2]$,

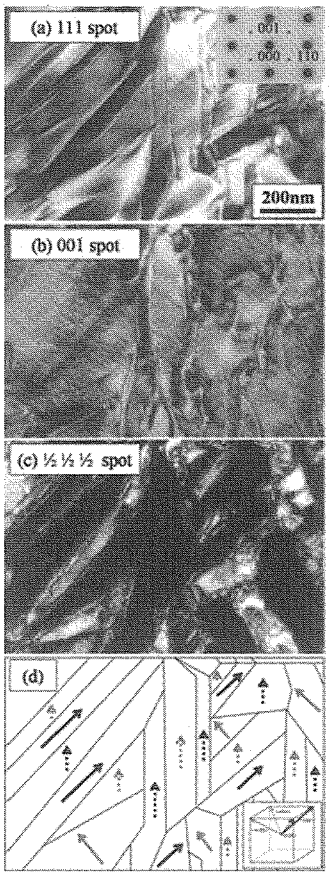

Figure 4. Ferroelectric domain structure in the x = 0.25 compound. (a) $g = [111]$, (b) $g = [001]$ and (c) $g = [1/2\ 1/2\ 1/2]$. (d) Schematic description of the FE domain configuration determined in this work.

respectively. In the dark-field images shown in Figs. 3(b) and 3(c), the regions with the bright contrast correspond to the region in which the condition that the product of the g and P_s vectors is positive, $g \cdot P_s > 0$, is satisfied. We can determine the direction of P_s by obtaining dark-field images with various different g vectors. Figure 3(d) is a schematic description of the spatial configuration of P_s in the composition for x = 0.20.

As the $BaTiO_3$ concentration (x) increases in (1-x)$BiFeO_3$-x$BaTiO_3$, it is found that the average size of the FE domains is reduced and the width of the FE domains can be estimated to be approximately 100 nm for the composition x = 0.25. In addition, the boundaries between the adjacent domains are very diffuse in the x = 0.25 compound. Figure 4(a) displays the dark-field image obtained by using $g = [111]$ at the room temperature in the x = 0.25 compound. As can be understood in Fig. 4(a), the average size of the FE domains reduces to the 100 nm width. To determine the direction of P_s in each FE domains, we obtained dark-field images at room temperature by using various different g vectors. Figures 4(b) and 4(c) exhibit the microstructures obtained by using $g = (001)$ and $g = (1/2\ 1/2\ 1/2)$, respectively. In the dark-field images shown in Figs. 4(b) and 4(c), the regions with the bright contrast correspond to the region in which the condition that the product of the g and P_s vectors is positive, $g \cdot P_s > 0$, is satisfied. We can determine the spatial configuration

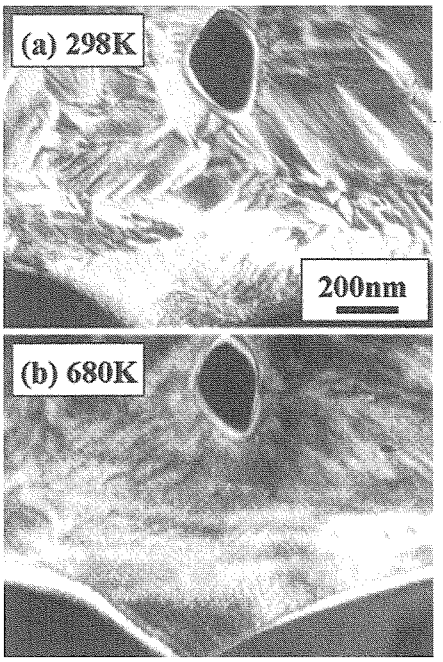

Figure 5. Temperature variation of the ferroelectric domain structure in the x = 0.28 compound. The images are obtained at (a) 298 K and (b) 680 K, respectively.

of the P_s by obtaining dark-field images with various different g vectors. Figure 4(d) is a schematic description of the spatial configuration of the P_s in the x = 0.20 compound.

To confirm that the microstructures obtained in Figs. 3 and 4 are associated with the FE domain structures, we investigated changes of the microstructures obtained by using $g = (111)$ as a function of the temperature in the wide temperature window between 298 K and 800 K in the x = 0.28 compound. Figure 5 shows the microstructures obtained at (a) 298 K and (b) 680 K, respectively. In Fig. 5(a) we can see FE domain structures clearly. As the temperature was increased to 700 K, it was found that the contrast due to the domain structures disappeared around 680 K, which corresponds to the ferroelectric transition temperature at 680 K [15]. This means that the domain structure shown in Fig. 5(a) corresponds to the FE domain structure.

4. Summary

In summary, we have clarified microstructures associated with the FE properties in (1-x)$BiFeO_3$-x$BaTiO_3$by the TEM experiments. It is revealed that structural change from the rhombohedral structure to the cubic one took place around the x = 0.33 compound at room temperature by partial substitution of $BaTiO_3$ for $BiFeO_3$. We examined the direction of P_s in each FE domains and found that the FE microstructures in the x = 0.28 compound are characterized as finely mixed states consisting of the FE domains with the various directions of the P_s.

Acknowledgment

This work was supported by Grant-in-Aid for Scientific Research on Priority Areas "Novel States of Matter Induced by Frustration" (19052002) from Ministry of Education, Culture,

Sports, Science and Technology. One of the authors (SM) was supported partially by the Murata Scientific Foundation.

References

1. N. A. Hill, *Annu. Rev. Mater. Res.* **32**, 1(2002).
2. C. W. Nan, *Phys. Rev. B* **50**, 6082(1994).
3. J. Wang, J. B. Neaton, H. Zheng, V. Nagarajan, S. B. Ogale, B. Liu, D. Viehland, V. Vaithyanathan, D. G. Schlom, U. V. Waghmare, N. A. Spaldin, K. M. Rabe, M. Wuttig, and R. Ramesh, *Sceince* **299**, 1719(2003).
4. S.-W. Cheong and M. Mostovoy, *Nat. Mater.* **6**, 13 (2007).
5. T. Kimura, T. Goto, H. Shintani, K. Ishizuka, T. Arima, and Y. Tokura, *Nature (London)* **426**, 55 (2003).
6. N. Hur, S. Park, P. A. Sharma, J. S. Ahm, S. Guha, and S-W. Cheong, *Nature (London)* **429**, 392(2004).
7. Th. Lottermoser, T. Lonkai, U. Amann, D. Hohlwein, J. Ihringer, and M. Fiebig, *Nature (London)* **439**, 541,(2004).
8. M. Fiebig, Th. Lottermoser, D. Frohlich, A. V. Goltsev, and R. V. Pissarev, *Nature (London)* **419**, 818 (2002).
9. T. Goto, T. Kimura, G. Lawes, A. P. Ramirez, and Y. Tokura, *Phys. Rev. Lett.* **92**, 257201(2004).
10. T. Zhao et al., *Nat. Mater.* **5**, 823(2007).
11. V. G. Bhide and M. S. Multani, *Solid State Commun.* **3**, 271 (1965).
12. J. M. Moreau, C. Michel, R. Gerson, and W. J. James, *J. Phys. Chem. Solids* **32**, 1315 (1971).
13. Y. N. Venevtsev and V. V. Gagulin, *Inorg. Mater.* **31**, 797 (1995).
14. P. Ravindran, R. Vidya, A. Kjekshus, and H. Fjellvag, *Phys. Rev. B* **74**, 224412 (2006).
15. M. M. Kumar, A. Srinivas and S. V. Suryarayana, *J. Appl. Phys.* **87**, 855 (2000).